Development of small Silicon modulators in Silicon-On-Insulator (SOI)

C.E. Png[a*], G.T. Reed[a], R.M.H. Atta[b], G. Ensell[b], A.G.R. Evans[b]
[a]School of Electronics and Physical Sciences, University of Surrey, Guildford GU2 7XH UK
[b]Department of Electronics and Computer Science, University of Southampton, SO17 1BJ UK

ABSTRACT

Silicon-based optical modulators are expected to be important components in some optical networks. The optical modulation mechanism can be achieved either via the plasma dispersion effect, or by thermal means. Both are relatively slow processes when utilized in large (multi micron) waveguide structures, which researchers tend to concentrate on for ease of coupling. Using large waveguide structures limits the operating speed and hence excludes the applicability of these devices in areas where higher speeds are required. This limitation could be overcomed by using smaller waveguides (of the order of ~1μm). In this paper, we present the basic operating mechanism, design, and fabrication details of an optimum three terminal *p-i-n* diode based optical phase modulator based on Silicon-On-Insulator (SOI). The device was optimised via electrical and optical modeling and is predicted to operated at ~1.3GHz with a power reduction of 900%, as compared to previously published designs.

Keywords: optical phase modulator, carrier injection, Silicon-On-Insulator (SOI)

1. INTRODUCTION

Recently, integrated optics in Silicon-On-Insulator (SOI) has become interesting for a range of applications [1-3]. The main reasons why SOI has proven successful for integrated optics are: the material and the processing are relatively low cost with resulting waveguides having a loss as low as 0.15dB/cm [4], optical modulation devices can be fabricated in SOI, and silicon micromachining allows hybrid circuits to include sources and detectors. Moreover, any technological development in either silicon or in the associated electronics industry can readily be transferred to silicon based integrated optics.

Previously, the majority of researchers concentrated on SIMOX (Separation by IMplantation of OXygen) or BESOI (Bond and Etchback SOI) with silicon surface layer thicknesses of the order of several microns and hence resulting in low loss waveguides. In addition, this also allows reasonably efficient coupling to the waveguides by endfire coupling. However, optical phase modulators based on several micron overlayer thicknesses are limited to modulation bandwidths of the order of 10-20MHz [5, 6]. In order to increase the speed of these devices the dimensions of the waveguides upon which the modulators are based, and hence the overlayer thickness should be reduced [7]. The French company SOITEC have developed a technique known as 'Smart-Cut' which is capable of producing SOI with flexibility and control of both the surface silicon layer thickness and the buried oxide layer thickness [8]. The commercial name is 'Unibond'. Unibond provides suitable wafers for the fabrications of our higher speed lower power optical phase modulators and will be used here.

In this paper we report the design of a high speed, small geometry (0.98μm silicon layer) optical phase modulator based on the plasma dispersion effect. The design process utilised the two-dimensional semiconductor simulator from SILVACO [9]. As a result, an optimum three terminal *p-i-n* diode modulator structure around a rib waveguide was identified [10, 11] in terms of both the power efficiency and the operating speed. Fabrication details, including the limitations encountered, are given. However, coupling to a thin waveguide requires specialist couplers, such as dual grating-assisted directional couplers (DGADCs) which is discussed in detail elsewhere [12].

*j.png@surrey.ac.uk; fax ++ 44 (0)1483 534139; School of Electronics and Physical Sciences, University of Surrey, Guildford, Surrey, GU2 7XH, UK

Photonics Packaging and Integration III, Randy A. Heyler, David J. Robbins, Ghassan E. Jabbour, Editors, Proceedings of SPIE Vol. 4997 (2003) © 2003 SPIE · 0277-786X/03/$15.00

2. SIMULATION OF OPTICAL PHASE MODULATORS

2.1 Optimum phase modulator geometry and operation

Fig. 1 shows the optimised device structure to be considered in this paper. This optimum design has been arrived at after optimization via electrical and optical modelling [10, 11]. It is a lateral optical phase modulator integrated into a low loss SOI rib waveguide. The device has a symmetrical *p-i-n* structure where two n^+ regions are joined as a common cathode. It is referred to as *n-p-n* device for obvious reasons. Both *n* and *p* regions were modelled as highly doped regions with peak doping concentrations of 10^{20}atoms/cm^3 and is based around an overall silicon thickness of 0.98μm, etched rib waveguides 0.5μm wide with an etch depth of 0.48μm in order to satisfy the single-mode condition [13]. The oxide thickness was modelled to be 0.4μm which ensures sufficiently good optical confinement. The device relies on the principle of the free-carrier plasma dispersion effect to produce a refractive index change in the waveguiding region of the ribs.

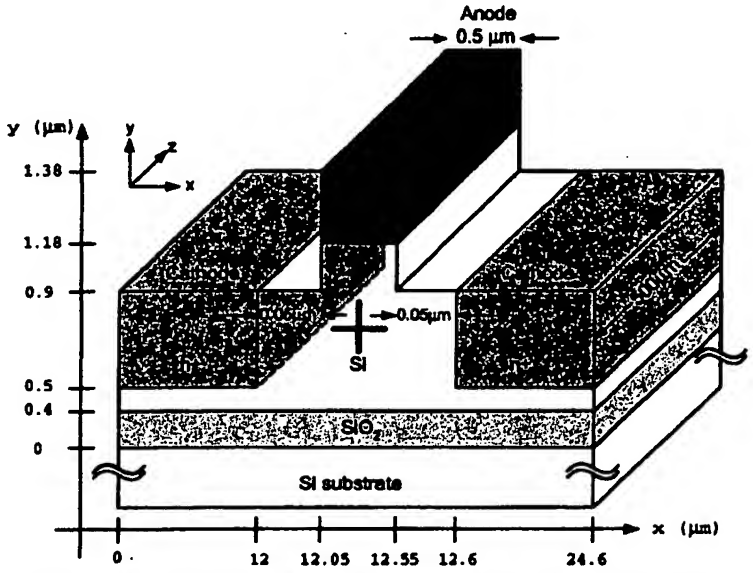

Fig. 1: Geometry of the optimum *p-i-n* phase modulator based on UNIBOND SOI.

When the anode is biased positively with respect to the cathode, such that the effective *p-i-n* diode structure is forward biased, both electrons and holes are injected into the guiding region, and hence the resultant phase of a propagating optical mode is altered by the associated change in refractive index. By including the modulator in a Mach-Zehnder interferometer (MZI) as shown in Fig. 2, interference fringes would be obtained when light is coupled into the device and compared with the reference path, i.e. optical intensity modulation is possible. When no bias is applied to the active arm of the MZI, the waves would combine constructively at the output of the MZI. If a π-phase shift is applied to the active arm, then the phase of the active arm would be 180° out-of-phase with respect to the reference arm and as a result, destructive interference results in a null output.

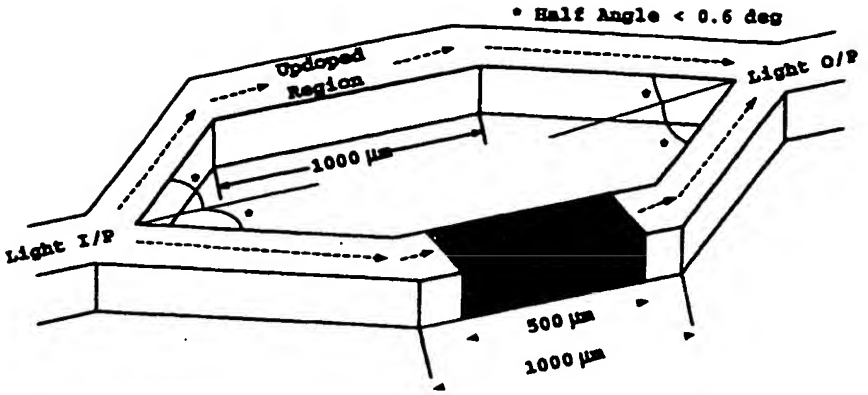

Fig. 2: Mach-Zehnder Interferometer (MZI) with the optimum *p-i-n* phase modulator.

2.2.1 Device Simulation - Electrical

The device was modelled for both its static and dynamic behaviour using the device simulation package from SILVACO [9]. The simulator is a physically based simulator which predicts the electrical characteristics associated with physical structures by solving the equations which describe semiconductor physics such as Poisson's equation and the charge continuity equations for holes and electrons. The simulator has been used to predict the injected free carrier concentrations in the intrinsic region of the devices for both dc and transient biasing conditions. The concentration of free carriers is then converted to refractive index change in the device by using the relations determined by Soref and Bennett [14]. The forward biased current-voltage characteristic of the device obtained from SILVACO is plotted in Fig.3, for three different devices. The difference between these devices is discussed later in this paper. To determine the voltage associated with a π-phase shift, the concentration of free carriers must be known. Assuming a uniform change in refractive index, the active device length required to produce the refractive index change associated with a π-phase shift is obtained approximately from

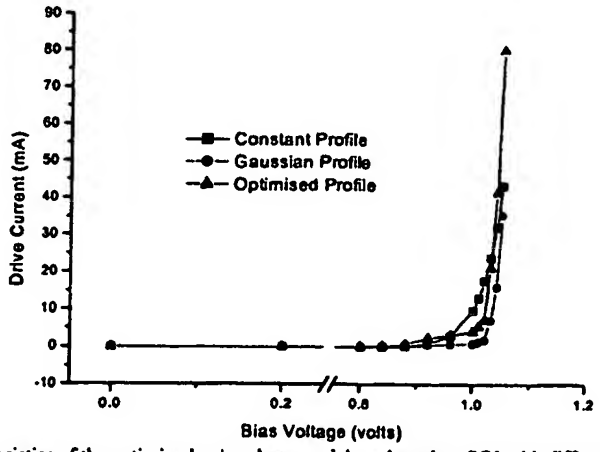

Fig. 3: IV characteristics of the optimized *p-i-n* phase modulator based on SOI with different doping profiles.

$$\Delta n = \frac{\lambda}{2L_g} \tag{1}$$

where L_g is the active length of the modulator. The concentration of injected carriers required to produce such a refractive index variation was quantified by Soref and Bennet [15] whom empirically determined the refractive index change as a function of free carriers in silicon via a Kramers-Kronig transformation of experimental data. At 1.55μm, which is also the operating wavelength where all the simulations here are based, the refractive index change (Δn) and the absorption change ($\Delta\alpha$) is given by

$$\Delta n = \Delta n_e + \Delta n_h = -[8.8 \times 10^{-22} \cdot (\Delta N_e) + 8.5 \times 10^{-18} \cdot (\Delta N_h)^{0.8}] \tag{2}$$

$$\Delta \alpha = \Delta \alpha_e + \Delta \alpha_h = 8.5 \times 10^{-18} \cdot (\Delta N_e) + 6.0 \times 10^{-18} \cdot (\Delta N_h) \tag{3}$$

where Δn_e is the change in refractive index change resulting from the change in free electron concentrations; Δn_h is the change in refractive index resulting from the change in free hole concentrations; $\Delta \alpha_e$ is the change in absorption resulting from change in free electron concentrations; and $\Delta \alpha_h$ is the change in absorption resulting from change in free hole concentrations. With an active length of 500μm, the required refractive index change, dictated by (2), is calculated to be 1.55×10^{-3} and applying this to (2), the required carrier injection concentration is approximately $4.6 \times 10^{17}/cm^3$, assuming equal numbers of electrons and holes. The validity of this assumption has been demonstrated by agreement between previous modelling and experimental results [6]. Since, the free carrier concentrations are approximately constant in the region of the optical mode, it is not necessary to evaluate the overlap integral between the optical mode and the free carriers. All simulations were based upon devices having an interaction length of 500μm and operating at a wavelength of 1.55μm. Fig. 4 shows the dc results for a device with a constant doping profile (-■-) in the contacts at the side of the rib. However, the drawback associated with a constant profile is that it is rather difficult to fabricate. A more realistic profile would be that of a gaussian distributed doping profile. Hence to make a qualitative comparison, results are also shown for a similar device with a gaussian doping profile (-●-). Also included is an optimized profile (-▲-), which gives the best performance. As will be presented, if the intended optimised device is compared to the device with a gaussian profile, there is a huge degradation in the device performance.

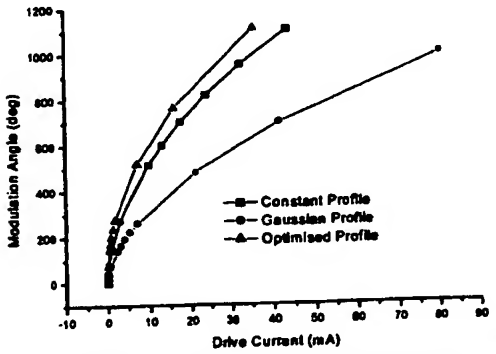

Fig. 4: Predicted dc performance for the optimised modulator using various doping profiles.

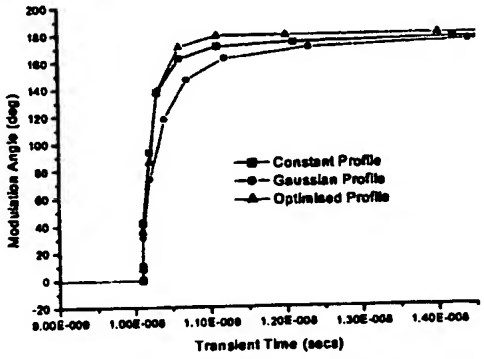

Fig. 5: Predicted transient performance for the optimised modulator using various doping profiles.

A typical measure of the quality of such devices is the drive current or current density required to achieve 180° phase shifts. From Fig. 4, the predicted drive current for the device with a constant doping profile is 1.5mA. However, a real device would probably have a different dopant distribution. Here a gaussian profile is again used by way of example. For a device with gaussian doping profile, the predicted drive current is 3.7mA. This implies a serious degradation of more than 100%. Consequently, an optimised fabrication technique was developed using conventional fabrication

processes that results in a predicted drive current of only 0.7mA. To demonstrate just how good this performance is, it is instructive to compare these results with those of Tang et al. [6], produced in 1995 and yet to be surpassed in terms of dc performance. Those devices operated with drive currents in the order of 7mA. Therefore, we would obtain over 900% dc improvement by considering the dc result of the optimised profile against Tang's result.

Fig. 5 shows the transient results for devices with the same three side doping profiles. For the transient solutions, the device anode and cathode were first zero biased for 10ns, followed by a step increase to V_π for 200ns, and finally a step decrease to 0V. In each case, V_π is the voltage corresponding to a 180° phase shift. The rise time t_r is defined as the time required for the induced phase shift to change from 10% to 90% of the maximum value, and the fall time t_f is defined as the time required for the induced phase shift to change from 90% to 10% of the maximum value. The rise time is considered as it is slower than the fall time and hence the limiting transition. From Fig. 5, the predicted rise times are 0.38ns, 0.51ns, and 1.08ns for the optimized, constant, and gaussian profiles respectively. To translate the rise time to the device operating speed, a factor of 0.5 is multiplied by the inverse of the rise time. Using the result provided by the optimized profile, we obtain a modulation bandwidth of more than 1.3GHz. This represents an improvement of over 10,000% improvement when compared to devices reported in the literature as having a typical speed of 13MHz (e.g. [5]). The results discussed thus far are summarised in Table 1 below.

Table 1: DC and transient characteristics for the optimised *p-i-n* optical phase modulator with various doping profiles.

Doping Type	Rise Time, t_r (ns)	Fall Time, t_f (ns)	Speed (GHz)	Drive Current, I_π (mA)
Constant	0.51	0.14	0.98	1.48
Gaussian	1.08	0.14	0.46	3.72
Optimised	0.38	0.13	1.30	0.70

2.2.2 Device Simulation - Optical

In order to ensure that the device is to operate with only a single mode, it was also modelled to determine the 2-dimensional (2D) optical field using BeamPROP [15], a commercial simulation package employing the beam propagation method (BPM) to solve high refractive index contrast waveguide. The modelling of the optimum *p-i-n* phase modulator is based on the geometry shown in Fig. 1. In this section we consider the optical power confinement in the waveguide geometry discussed in the previous section. The doping region at either side of the rib of the phase modulator is doped

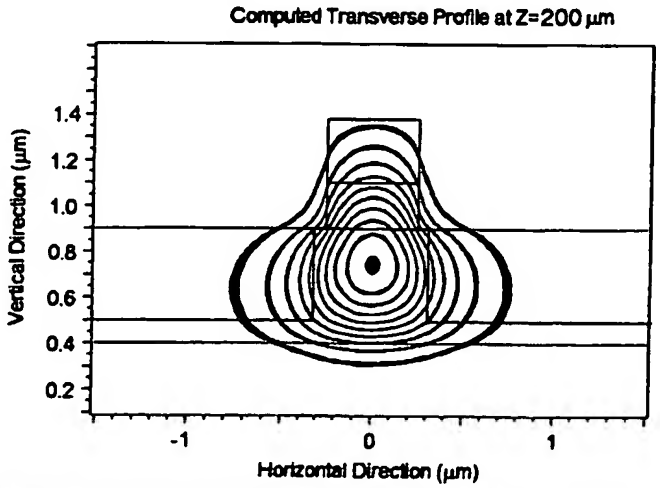

Fig. 6: Optical power confinement. Contours are in increasing intensity towards waveguide center.

with a constant doping profile of $10^{20}/cm^3$, which causes a decrease of refractive index (Δn=–0.173) in this doped region [14]. In addition to acting as the device contact, the doped region serves as a barrier to prevent optical power from leaking out, but the high doping profile close to the rib can potentially also result in an increase in absorption loss. The simulation result in Fig. 6 shows the computed fundamental mode profile after a propagation distance of 200μm. The optical power is well confined in the rib region and demonstrates single mode operation. However, it is also obvious that some power is contained within the sidewall contacts. If we move the contacts laterally to avoid absorption, the speed of the device is compromised. Hence design is partially a trade off between optical loss and operating speed.

3. FABRICATION

3.1 Fabrication of the proposed device in SOI

In the previous section, the optical phase modulator design was described. Fabrication of this device is currently underway at Southampton University, together with a number of other design variants. Fig. 7 shows a Scanning Electron Microscopy (SEM) picture of the rib waveguide, demonstrating the realisation of the device. In order to couple light into the waveguide efficiently, we need to integrate grating couplers into the input of the optical phase modulator. Fig. 8 shows an SEM image of such a coupler. More details about the coupler could be obtained from previous publications [10, 16].

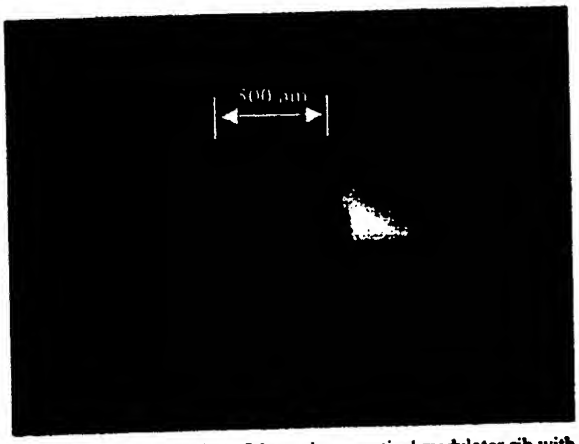

Fig. 7: SEM image for the cross-section of the optimum optical modulator rib with its sidewalls.

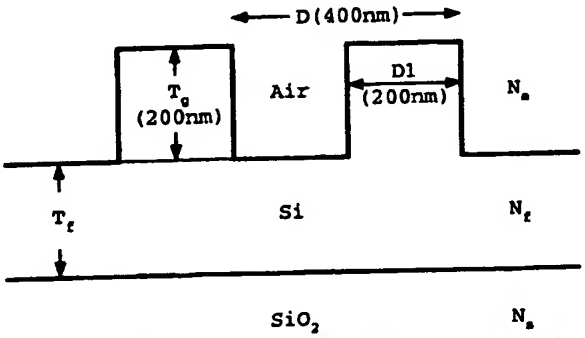

Fig. 8: Sketch of the grating couplers at the end of the rib waveguide.

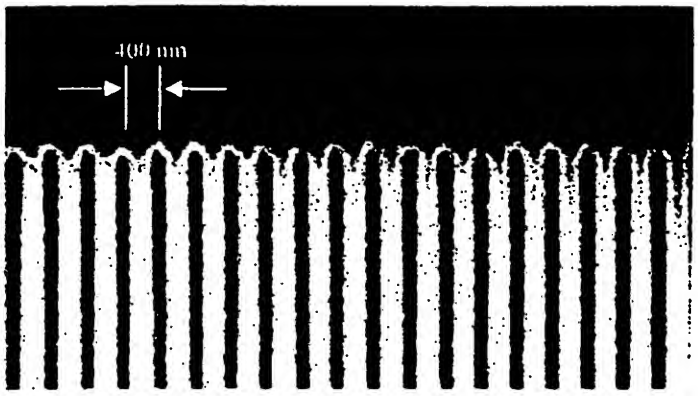

Fig. 9: SEM image of the grating couplers at the end of the rib waveguide with 400nm pitch.

Fabrication of the idealized device shown in Fig. 1 is difficult due primarily to dopant introduction and redistribution under thermal processing, but should be possible using high resolution lithography and very slow oxide mask deposition. Consequently, we are currently fabricating a slightly different device geometry which will demonstrate the principles of our design strategy. Fig. 10 shows preliminary data for the measured electrical characteristic for the optical modulator between the rib and the sides for the fabricated device of Fig. 7.

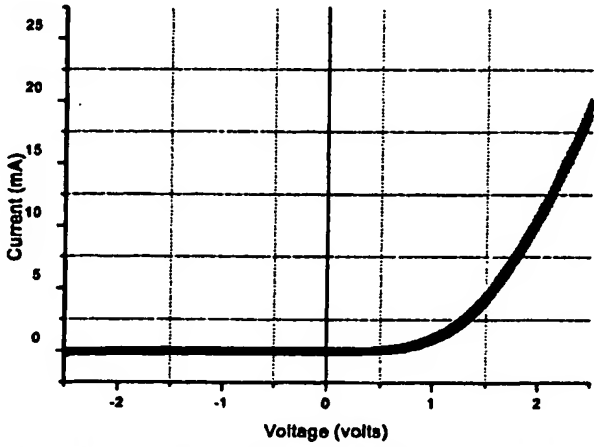

Fig. 10: Measured electrical characteristic for the optical modulator between the rib and the sides for the fabricated device in Fig. 7. The I/V characteristics show that there is no short circuit between the rib and the sides.

4. CONCLUSION

We have presented the design of a high speed optical phase *p-i-n* modulator based on SOI. The design was optimised both electrically and optically for switching speed and power consumption, and are predicted to offer state-of-the-art improvements in device performances. Fabrication details to date, including preliminary results are also presented. This optimum optical phase modulator is predicted to offer an improvement of device speed of over 10,000% at ~1.3GHz

and a drive current reduction of 900% at 0.7mA. In order to couple light to this modulator, a grating coupler in SOI or a dual grating-assisted directional coupler (DGADC) can be used.

ACKNOWLEDGEMENTS

C.E. Png is grateful to Bookham Technology plc and for an Overseas Research Student (ORS) Award Scheme for funding his Ph.D. studies. All authors are grateful to EPSRC in the UK for funding, and to SOITEC, France for provision of SOI wafers.

REFERENCES

1. A. G. Rickman, G. T. Reed, and F. Namavar, "Silicon-on-insulator optical rib waveguide loss and mode characteristics", *IEEE J. Lightwave Technol.*, **12**, pp. 1771-1776, 1994.
2. A. G. Rickman, and G. T. Reed, "Silicon-on-insulator optical rib waveguides: low mode characteristics, bends and y-junctions", *IEE Proc-Op. Lightwave Technol.*, **12**, pp. 1394-1400, 1994.
3. J. Schmidtchen, A. Splett, B. Schuppert, and K. Petermann, "Low-loss single-mode optical waveguides with large cross section in silicon-on-insulator", *Elect. Lett.*, **27**, pp. 1486-1487, 1991.
4. T. W. Ang, P. D. Hewitt, A. Vonsovici, G. T. Reed, A. G. R. Evans, P. R. Routley, T. Blackburn, and M. R. Josey, "Integrated Optics in Unibond for greater flexibility", *Electrochemical Society Proc.*, **99-3**, pp. 353-360, 1999.
5. P. D. Hewitt, and G. T. Reed, "Improving the response of optical phase modulators in SOI by computer simulation", *J. Lightwave Technol.*, **18**, pp. 443-450, 2000.
6. C. K. Tang, and G. T. Reed, "Highly efficient optical phase modulator in SOI waveguides", *Elect. Lett.*, **31**, pp. 451-452, 1995.
7. A. Vonsovici, and A. Koster, "Numerical simulation of a silicon-on-insulator waveguide structure for phase modulation at 1.3 μm", *J. Lightwave Technol.*, **17**, pp. 1-7, 1999.
8. Auberton-Herve, A.J., Bruel, M., Aspar C. Maleville, B. and Moriceau, H., "Smart-Cut®: the basic fabrication process for Unibond® SOI wafers", *IEICE Trans. Elect.*, 1997, **E80 C**, 3, pp.358-363.
9. SILVACO International, 4701 Patrick Henry Drive, Bldg 1, Santa Clara, California.
10. C. E. Png, G. Masanovic, and G. T. Reed, "Coupling to 1μm Silicon Modulators", *Proc. SPIE*, **4654**, pp 62 – 69, 2002.
11. C. E. Png, G. Masanovic, S. P. Chan, S. T. Lim, G. T. Reed, and A. Vonsovici, "Over 7500% increase in device speed for optical phase modulators in silicon", PREP 2002, West Midlands Conference Centre, Nottingham Uni.
12. G. Masanovic, C. E. Png, V. Passaro, G. T. Reed, R. M. H. Atta, and A. G. R. Evans, "Coupling from optical fibres to fast silicon modulators", accepted for publication SPIE Photonics West Jan 2003.
13. R. A. Soref, J. Schmidtchen, and K. Petermann, "Large single-mode rib waveguides in GeSi-Si and Si-on-SiO_2", *IEEE J. Quantum Electron.*, **27**, pp. 1971-1974, 1991.
14. R. A. Soref, and B. R. Bennet, "Kramers-Kronig analysis of E-O switching in silicon", *SPIE Integrated Opt. Circuit Eng.*, **704**, pp. 32-37, 1986.
15. RSoft, Inc. *Research Software*, 200 Executive Boulevard, Ossining, NY 10562.
16. T. W. Ang, G. T. Reed, A. Vonsovici, A. G. R. Evans, P. R. Routley, M. R. Josey, "Effects of grating heights on highly efficient Unibond SOI waveguide grating couplers", *IEEE Photon. Technol. Lett.*, **12**, pp. 59-61, 2000.